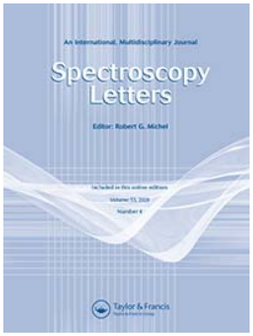

Spectroscopy Letters

An International Journal for Rapid Communication

ISSN: 0038-7010 (Print) 1532-2289 (Online) Journal homepage: https://www.tandfonline.com/loi/lstl20

A combined experimental and theoretical study on vibrational spectra of 3-pyridyl methyl ketone

Sibel Celik, Meryem Alp & Senay Yurdakul

To cite this article: Sibel Celik, Meryem Alp & Senay Yurdakul (2020) A combined experimental and theoretical study on vibrational spectra of 3-pyridyl methyl ketone, Spectroscopy Letters, 53:4, 234-248, DOI: 10.1080/00387010.2020.1734840

To link to this article: https://doi.org/10.1080/00387010.2020.1734840

SPECTROSCOPY LETTERS
2020, VOL. 53, NO. 4, 234–248
https://doi.org/10.1080/00387010.2020.1734840

Taylor & Francis
Taylor & Francis Group

A combined experimental and theoretical study on vibrational spectra of 3-pyridyl methyl ketone

Sibel Celik[a], Meryem Alp[b] and Senay Yurdakul[b]

[a]Department of Health Care Services, Ahi Evran University, Kırşehir, Turkey; [b]Department of Physics, Gazi University, Ankara, Turkey

ABSTRACT

Using some spectral methods and density functional theory calculations, a complete structural, vibrational, thermodynamic, electronic, nonlinear optical properties of 3-pyridyl methyl ketone have been evaluated. The Fourier transform infrared spectrum was obtained for the title molecule at room temperature. In the theoretical calculations, the Becke three Lee-Yang-Parr functional with 6-311++G(d,p) basis set was applied to carry out the quantum mechanical calculations. The infrared spectra were interpreted by using of normal coordinate analysis based on the scaled quantum mechanical force field. In addition, molecular electrostatic potential map, some thermodynamic parameters at different temperatures of compound were investigated.

ARTICLE HISTORY
Received 13 September 2019
Accepted 21 February 2020

KEYWORDS
DFT; electronic properties; 3-pyridyl methyl ketone; vibrational spectra

Introduction

3-Pyridyl methyl ketone (3-pmk), also known as methyl β-pyridyl ketone, is an analog of nicotinic acid (niacin) containing a methyl group in place of the hydroxyl.[1]

Pyridines represent class of compounds that can significantly contribute to the organoleptic properties of foods.[2,3] Especially, methyl-pyridyl ketones are known as aroma components of foods, perfumes, and smoking suppressants, showing several biological activities and constituting part of the structure of some important biologically active compounds.

Uwai et al.[4] purified and identified the enzyme that catalyzes the stereo selective reduction of methyl-pyridyl ketones in the rat liver, because the liver is the main internal organ for drug metabolism and contains plenty of enzymes.

The absorption and luminescence characteristics of methyl-pyridyl ketones have been examined in polar and nonpolar media at room temperature and low temperature (77 K).[5]

Although its industrial and medical importance, the structure and vibrational spectroscopic analysis for 3-pyridyl methyl ketone are limitedly reported, and the crystal structure and vibrational spectroscopic study of pure vibrational spectroscopic molecule are still unavailable. On the other hand, Medhi[6] determined and empirically assigned the Infrared (IR) and Raman bands of methyl-pyridyl ketones in 1977. Sett et al.[7] have assigned again these bands using empirical force fields based on pyridine ring and ethanoyl group approximation.

Although extensive research has been carried out within the relevant literature, no single study exists on experimental and theoretical examination of the isolated 3-pmk molecule. To elaborate the vibrational and some electronic properties of 3-pmk, as an important compound in the scientific research, FT-IR spectrum has been recorded and calculated theoretical vibrational spectra, molecular structure, and some electronic properties.

Within the current study, special attention was paid the theoretical calculations that made it possible to obtain molecular structure and vibrational spectra for comparison with experimental data. The main body of the article is divided into many sections. In section Computational methods, the optimized molecular structure will be

CONTACT Senay Yurdakul senayy@gazi.edu.tr Department of Physics, Gazi University, Ankara, Turkey.

presented. Section Assignment of vibrational spectra presents the theoretical and experimental vibrational spectroscopic data. In section Molecular orbital analysis and density of state, the Highest Occupied Molecular Orbital (HOMO), the Lowest Unoccupied Molecular Orbital (LUMO), and simulated density of states spectrum (DOS) will be presented. Next section deals with the molecular electrostatic potential. The thermodynamic parameters for 3-pmk were discussed in section Thermodynamic properties, whereas the polarizability and hyperpolarizability of 3-pmk were presented in section Non-linear optical properties. In sections Fukui functions and Charge analysis, Fukui functions, and charges will be presented, respectively.

Computational methods

Density functional theory (DFT) computations for the geometric optimization and frequency calculation were conducted using Gaussian 09 program.[8] The calculations employed the B3LYP exchange-correlation functional, which combines the hybrid exchange functional of Becke[9] with the gradient-correlation functional of Lee et al.[10] and the split-valence polarized 6-311++G(d,p) basis set. Molecular geometries were fully optimized by the Berny algorithm. The optimal geometry was determined by minimizing the energy with respect to all geometrical parameters without imposing molecular symmetry constraints. In the optimized structure, imaginary frequency modes were absent which provided a true minimum picture of the potential energy surface (Fig. 1).

Following the geometry optimizations with B3LYP method, the optimized structural parameters were used in the vibrational wavenumber calculation at DFT level to characterize all stationary points while minima. Total Energy Distribution (TED) values were obtained by using the Parallel Quantum Solutions software.[11] In addition, the frontier molecular orbital analysis and density of state analysis were conducted. In order to the support the hydrogen bonding studies, Fukui function, natural bond orbital (NBO) analysis, and molecular electrostatic potential (MEP) calculations were conducted.

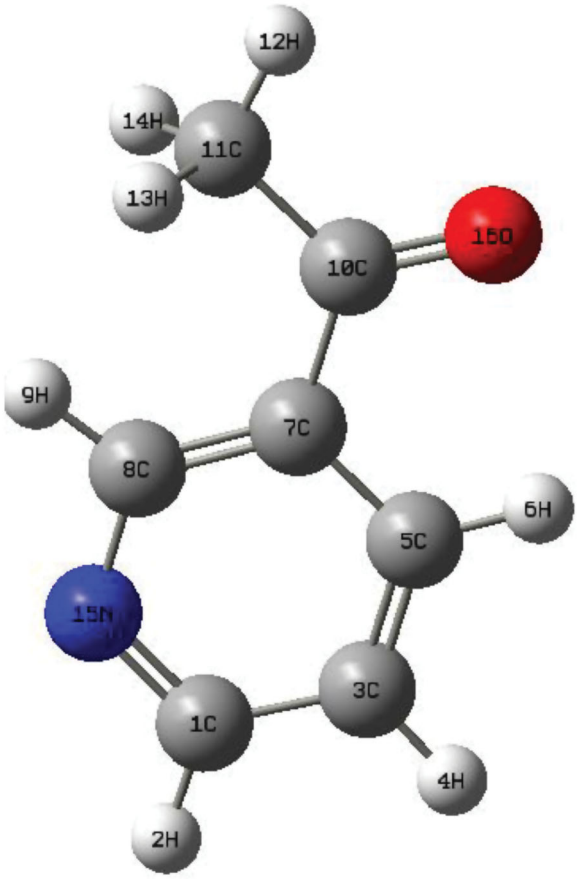

Figure 1. Optimized molecular structure of 3-pyridyl methyl ketone at Becke three Lee-Yang-Parr/6-311++G(d,p) level of theory. The optimized structure gives the minimum energy obtained for the molecule.

Experimental details

3-Pyridyl methyl ketone was attained from Aldrich and used without further purification. FT-IR spectrum was observed between 3500 and 550 cm^{-1} on a Bruker Vertex 80 spectrometer equipped with a Pike MIRacle ATR accessory. The Far-IR spectrum was recorded between 600 and 100 cm^{-1} on JASCO FTIR-6800 Series system.

Result and discussion

Molecular structure

The optimized molecular structure of the 3-pyridyl methyl ketone with atomic numbering is shown in Fig. 1. The theoretical geometrical parameters were calculated DFT/B3LYP level of theory with the 6-311++G(d,p) basis set. The geometrical values (bond lengths and bond angles) and X-ray data are presented in Table 1.

Table 1. Optimized geometrical parameters (bond lengths and bond angles) of 3-pyridyl methyl ketone by Becke three Lee-Yang-Parr/6-311++G(d,p) in comparison with experimental X-ray diffraction data.

	Bond lengths (Å)			Bond angles (°)	
Parameters	Calc	XRD[a]	Parameters	Calc.	XRD[a]
$C_1 - H_2$	1.084	0.950	$H_2 - C_1 - C_3$	120.4	118.9
$C_1 - C_3$	1.386	1.381	$H_2 - C_1 - N_{15}$	116.0	118.8
$C_1 - N_{15}$	1.335	1.351	$C_3 - C_1 - N_{15}$	123.5	122.1
$C_3 - H_4$	1.083	0.950	$C_1 - C_3 - H_4$	120.2	120.5
$C_3 - C_5$	1.386	1.381	$C_1 - C_3 - C_5$	118.4	119.0
$C_5 - H_6$	1.083	0.950	$H_4 - C_3 - C_5$	121.2	120.5
$C_5 - C_7$	1.400	1.396	$C_3 - C_5 - H_6$	122.0	120.4
$C_7 - C_8$	1.400	1.396	$C_3 - C_5 - C_7$	119.0	119.2
$C_7 - C_{10}$	1.501	1.504	$H_6 - C_5 - C_7$	119.0	120.3
$C_8 - H_9$	1.085	0.951	$C_5 - C_7 - C_8$	117.6	118.3
$C_{10} - C_{11}$	1.515	1.492	$C_5 - C_7 - C_{10}$	119.2	119.6
$C_{10} - O_{16}$	1.216	1.215	$C_8 - C_7 - C_{10}$	123.1	122.0
$C_{11} - H_{12}$	1.088	0.980	$C_7 - C_8 - H_9$	120.7	118.7
$C_{11} - H_{13}$	1.094	0.980	$C_7 - C_8 - N_{15}$	124.0	122.4
$C_{11} - H_{14}$	1.094	0.980	$H_9 - C_8 - N_{15}$	115.3	118.8
$C_8 - N_{15}$	1.335	1.344	$C_7 - C_{10} - C_{11}$	118.8	118.2
RMSD	0.083		$C_7 - C_{10} - O_{16}$	120.1	118.6
			$C_{11} - C_{10} - O_{16}$	121.0	122.9
			$C_{10} - C_{11} - H_{12}$	108.7	109.4
			$C_{10} - C_{11} - H_{13}$	110.8	109.4
			$C_{10} - C_{11} - H_{14}$	110.8	109.4
			$H_{12} - C_{11} - H_{13}$	109.4	109.4
			$H_{12} - C_{11} - H_{14}$	109.4	109.5
			$H_{13} - C_{11} - H_{14}$	107.4	109.4
			RMSD	1.480	

Å: Angstrom; °: degree.
[a]Taken from Ref. [12].

Also, calculated parameters were compared with X-ray data for bis (3-pyridyl methyl ketone)-bis(isothiocyanato)-zinc(II),[12] due to the fact that crystallographic data are not available yet for the title molecule.

As shown in Table 1, the optimized parameters are in good agreement with the experimental data. The bond lengths and bond angles comparisons were expressed in terms of root-mean-square deviations (RMSD) values bond lengths (0.083) and the bond angles (1.480) the B3LYP method with the 6-311++G(d,p) basis set.

The bond lengths of all C–C bond in the pyridine ring were found to be 1.386–1.400 Å computationally and 1.381 Å–1.396 Å experimentally, which signifies that there is no demarcation of single or double bond in the pyridine ring. In addition to the bond length, C–C in pyridine ring is equal and almost close to experimental value, but these values largely differ from the C–C bond length within ethanoyl group where the computational value is 1.515 Å and the experimental value is approximately 1.492 Å. The C–C bond lengths in the pyridyl ring are shorter than bond lengths in ethanoyl group due to inductive electron effect which may tend to lengthen the bond.

The C–N bond lengths in pyridine ring were found almost equal around 1.335 Å, very closer to experimental value 1.351 Å. In particular, C–O bond length is in good agreement with the calculated value.

The C–H bond length values are experimental at 0.950 Å to 0.980 Å, which are smaller than the calculated C–H (ring) and C–H (ethanoyl group) values are 1.084 Å–1.094 Å, respectively.

As can be seen from Table 1, the calculated bond angle values are very close experimental bond angle values. In particular, C–C–C, C–C–H, and H–C–H bond angles are in very good agreement with the XRD data. However, small deviations were observed in the harmony between the theoretical and experimental bond angle values of C–C–N and H–C–N bond angles. These small deviations can be explained by the fact that the calculations relate to the isolated molecule, where intermolecular Coulombic interactions with the neighboring molecules are absent, whereas the experimental results correspond to interacting molecules in the crystal lattice.[13]

Assignment of vibrational spectra

The recorded FT-IR bands and scaled wavenumbers along with TED are presented in Table 2. The comparison of computed and experimental FT-IR and Far-IR spectra are shown in Fig. 2. The DFT hybrid B3LYP functional tends to overestimate the fundamentals modes, therefore, proper scale factor of 0.997 for the wavenumber less than 1800 cm^{-1} and 0.955 above 1800 cm^{-1}[14,15] were applied to B3LYP/6-311++G (d,p) method by least square method as tabulated in Table 2. As a result of neglecting the anharmonicity in real system, comparison of the wavenumbers calculated at B3LYP with the experimental values reveals the overestimation of the calculated vibrational modes.

The hetero-aromatic structure shows the presence of the C–H stretching vibrations in the region 3100–3000 cm^{-1}, which is characteristic region for the ready identification of the C–H stretching vibrations.[16] The pyridine ring has

Table 2. Calculated vibrational wavenumbers, frequencies, scaled frequencies, normalized absorption intensities of the infrared and Raman spectrum and observed infrared frequencies, and their detailed assignments with total energy distribution(%) for 3-pyridyl methyl ketone.

		Calculated			Observed	
Mode	Fre	Fre[a]	I_{IR}[b]	I_{RA}[b]	IR	%TED[c]
ν_{42}	3200	3056	3.2	100	–	80 υ_{CH}(py)
ν_{41}	3184	3041	3.3	100	3048vw	78 υ_{CH}(py)
ν_{40}	3163	3021	4.5	51.5	–	68 υ_{CH}(py)
ν_{39}	3153	3011	7.2	100	–	75 υ_{CH}(py)
ν_{38}	3144	3003	5.9	100	–	76 υ_{CH}(ethanoyl)
ν_{37}	3092	2953	3	57.4	–	80 υ_{CH}(ethanoyl)
ν_{36}	3034	2897	1	62.9	–	88 υ_{CH}(ethanoyl)
ν_{35}	1750	1746	100	73.4	1684vs	20 υ_{CO} + 13 υ_{CC} + 13 δ_{CCH}
ν_{34}	1625	1621	49.5	100	1583s	28 υ_{CC} + 18 δ_{CCH} + 13 δ_{CCC} + 12 δ_{HCC}
ν_{33}	1604	1600	9.1	14	–	23 υ_{CC} + 13 δ_{HCN} + 17 δ_{HCC}
ν_{32}	1507	1504	1.1	4.8	–	15 υ_{CC} + 24 δ_{CCH} + 18 δ_{HCC}
ν_{31}	1479	1476	8.9	15.5	1473w	25 δ_{HCH} + 25 Γ_{CCCH} + 25 Γ_{OCCH}
ν_{30}	1471	1468	7.1	11.3	–	37 δ_{HCH} + 20 Γ_{CCCH} + 20 Γ_{OCCH}
ν_{29}	1447	1444	28.6	5.7	1417s	15 υ_{CC} + 17 δ_{HCC} + 13 δ_{HCN}
ν_{28}	1391	1388	35.5	3.7	1359s	32 δ_{CCH} + 32 δ_{HCH}
ν_{27}	1359	1356	1.4	1.3	–	26 δ_{CCH} + 16 δ_{CCC} + 17 δ_{HCN}
ν_{26}	1294	1291	23	11.8	1304vw	16 υ_{CN} + 30 υ_{CC}
ν_{25}	1278	1275	100	36.9	1268vs	23 υ_{CC} + 14 δ_{CCH}
ν_{24}	1224	1221	28.8	15.3	1194m	11 υ_{CN} + 13 υ_{CC} + 14 δ_{CCH} + 15 δ_{HCN} + 22 δ_{HCC}
ν_{23}	1136	1134	55.9	2.3	1118m	24 δ_{CCH} + 21 δ_{HCC}
ν_{22}	1101	1099	7.9	9.3	1093m	18 υ_{CC} + 17 δ_{CCH} + 13 δ_{HCC}
ν_{21}	1055	1053	0	100	–	24 υ_{CC} + 11 υ_{CN} + 13 δ_{CCH} + 14 δ_{HCC}
ν_{20}	1046	1044	1.9	2.9	–	16 δ_{CCH} + 15 Γ_{CCCH} + 11 Γ_{OCCH}
ν_{19}	1038	1036	36.2	44	1021s	18 δ_{CCC} + 15 δ_{CCH} + 12 δ_{CCN}
ν_{18}	1014	1012	1.7	0	–	28 Γ_{HCCH} + 26 Γ_{HCCC} + 13 Γ_{CCCH}
ν_{17}	988	986	2.8	0	–	23 Γ_{HCCC} + 20 Γ_{HCCH} + 13 Γ_{CCCH} + 17 Γ_{HCNC}
ν_{16}	960	958	99.5	7.3	955s	16 υ_{CC} + 25 δ_{CCH} + 12 Γ_{CCCH} + 12 Γ_{OCCH}
ν_{15}	947	945	1.8	1.5	–	26 Γ_{CCCH} + 12 Γ_{HCCC} + 11 Γ_{HCCH} + 11 Γ_{HCNC}
ν_{14}	824	822	75.3	3	806s	13 Γ_{HCHC} + 14 Γ_{HCCC} + 14 Γ_{NCCH}
ν_{13}	763	761	7.5	100	750m	24 υ_{CC} + 10 δ_{CCN} + 13 δ_{HCC} + 11 δ_{CCC}
ν_{12}	717	715	100	3	701vs	12 Γ_{CCCH} + 13 Γ_{HCCC} + 12Γ_{CCCC} + 12 Γ_{HCNC}+12 Γ_{CCNC}
ν_{11}	639	638	50.1	77.4	624s	18 δ_{CCC} + 17 δ_{CCH} + 10 δ_{CNC}
ν_{10}	608	607	13.6	5.6	–	16 Γ_{CCCH} + 11 Γ_{CCCO} + 10 Γ_{OCCH}
ν_{9}	599	598	100	95.1	589vs	11 υ_{CC} + 14 δ_{CCC} + 19 δ_{CCO}
ν_{8}	461	460	11.1	36.3	465w	28 δ_{CCC} + 11 δ_{CCO}
ν_{7}	419	418	25.7	10.7	405m	12 Γ_{CCCH} + 15 Γ_{CCCC}
ν_{6}	387	386	4.6	0	–	12 Γ_{CCCH} + 11 Γ_{HCCC} + 11 Γ_{CCCN}
ν_{5}	366	365	13	100	367w	16 υ_{CC} + 16 δ_{CCN} + 21 δ_{CCC}
ν_{4}	214	214	100	8.5	219m	50 δ_{CCC} + 10 δ_{CCO}
ν_{3}	152	152	0.4	1.8	156m	45 Γ_{OCCH} + 45 Γ_{CCCH}
ν_{2}	150	150	5.4	100	135vw	23Γ_{CCCH} + 17 Γ_{CCCC} + 15 Γ_{CCCN}
ν_{1}	57	57	100	100	–	30 Γ_{CCCC} + 30 Γ_{CCCO} + 12 Γ_{OCCH}

ν: stretching; δ: in-plan bending; Γ: torsion; s: strong; m: medium; w: weak; v: very.
[a]Scaled wavenumbers calculated at B3LYP/ 6-311 G++(d,p) using scaling factors 0.997 for the wavenumber less than 1800 cm^{-1}, and 0.955 above 1800 cm^{-1}.[14,15]
[b]Relative absorption intensities and relative Raman intensities normalized with highest peak absorption equal to 100.
[c]Total energy distribution calculated B3LYP 6-311 G++(d,p) level, TED less than 10% are not shown.

the four CH stretching vibrations. 3056 cm^{-1}, 3041 cm^{-1}, 3021 cm^{-1}, and 3011 cm^{-1} peaks were predicted the CH stretching vibrations by the DFT calculation. According to the TED results, TED contributions were almost calculated as pure modes. Medhi et al.[6] reported that CH stretching vibrations of the pyridine ring were observed at 3031 cm^{-1}, 3047 cm^{-1}, 3066 cm^{-1}, and 3082 cm^{-1} in the FT-IR spectrum. Additionally, the CH stretching vibrations of the ethanoyl group were calculated at 3003 cm^{-1}, 2953 cm^{-1}, and 2897 cm^{-1} modes. Symmetric CH_3 vibration was calculated at 3027 cm^{-1} while the asymmetric CH_3 stretching vibration calculated at 3085 cm^{-1}, 3137 cm^{-1} by means of DFT calculation. One peak was detected at 3048 cm^{-1} in the FT-IR spectrum. Medhi et al.[6] reported that symmetric CH_3 stretching vibration measured at 2923 cm^{-1} in the FT-IR spectrum. The asymmetric CH_3 stretching vibrations were observed at 2972 cm^{-1} and 3009 cm^{-1} by means of FT-IR spectrum. The weak nature of aromatic C–H stretching vibration in the spectrum is due to the reduction of negative charge on carbon atoms, which leads to decrease in dipole moment. The reason of reduction is that the substituent

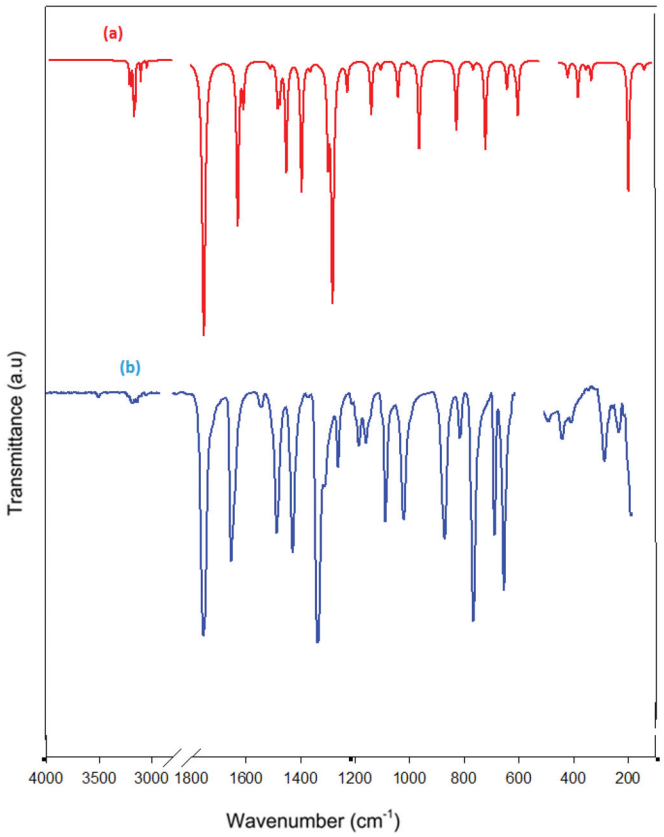

Figure 2. Comparison on theoretical (a) and experimental (b) Fourier Transform Infrared Spectrum of 3-Pyridyl methyl ketone at Becke three Lee-Yang-Parr/6-311++G(d,p), which represented on the transmittance (arbitrary unit) against the wavenumbers (1/centimeter). Experimental Far-Infrared spectrum of 3-pyridyl methyl ketone in the range 600–100 cm^{-1} on Jasco Fourier transform infrared-6800 series system. The experimental spectrum reveals the entire characteristic far-infrared spectrum.

withdraws more electrons from the carbon atoms which increase in chain length of the substituent.[17]

The C = O stretching vibration exhibits a strong band in the region 1600–1750 cm^{-1}.[18] For the 3-pmk, the symmetric stretching mode of C = O assigned at 1684 cm^{-1} (very strong) in the IR spectrum, theoretically calculated wavenumber and infrared intensity values were 1746 cm^{-1} and 100 in the DFT calculation, respectively.

The C–N vibrations of aromatic amines generally appear at 1342–1266 cm^{-1}. But they are not easy to assign those, because of several bands appear in the same region.[19] In the present study, these bands observed at 1304, 1194 cm^{-1} in the FT-IR spectrum and theoretically calculated at 1291, 1221 $cm^{-1}$are assigned to ring stretching, ring deformation together with C–N stretching modes.

In the experimental FT-IR spectrum, the δ_{HCH} band appeared at 1359 cm^{-1} (strong) and corresponds to the CH_3 asymmetric deformation vibration of the ethanoyl group of 3-pmk. The theoretical band was predicted at 1388 cm^{-1}, and detected at 1423 cm^{-1} in the FT-IR spectrum by Medhi et al.[6] In the ethanoyl group, the CH_3 functional groups possess the two asymmetric, one symmetric CH_3 stretching vibrations. Generally, stretching vibrations of methyl group are slightly lower than those of pyridine ring.

In line with this observation, the calculated frequencies at 1476, 1468, 1044, and 607 cm^{-1} are assigned to O–C–CH_3 angle bending vibrations. The C–C–O bending mode assigned at 589 cm^{-1} (very strong) in FT-IR spectrum, the corresponding theoretical values were calculated at 598, 460, and 214 cm^{-1}.

The Far-IR bands at 465(w) cm^{-1}, 219(m) cm^{-1}, and 367(w) cm^{-1} were assigned to C–C–C in-plane bending vibrations. These modes are calculated at 460 cm^{-1}, 214 cm^{-1}, and 365 cm^{-1}. The ethanoyl group torsions (CCCH, CCCC, and OCCH) were assigned at 405(m) cm^{-1} (calc. 418 cm^{-1}) and 156(m) cm^{-1} (calc. 152 cm^{-1}).

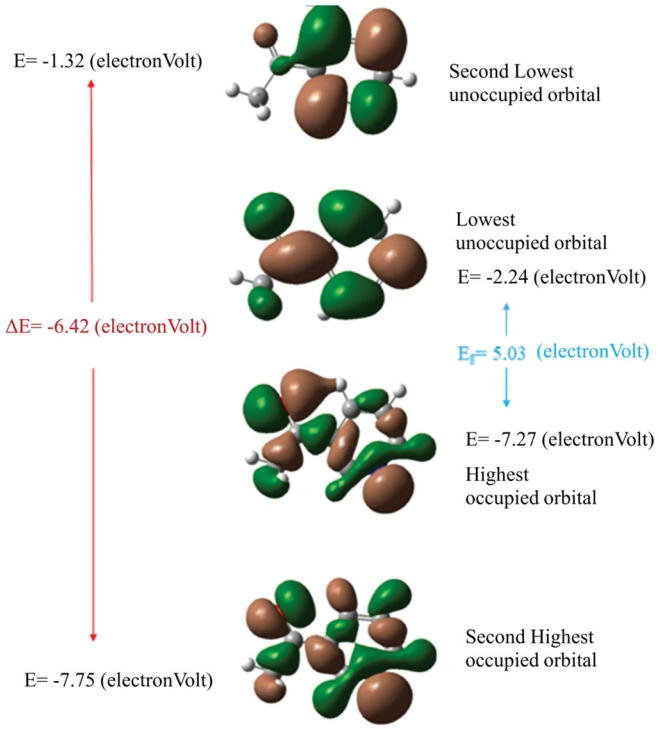

Figure 3. The calculated energy values (electronVolt) of the Highest Occupied Molecular Orbital and the Lowest Unoccupied Molecular Orbital of the 3-pyridyl methyl ketone molecule.

These experimental values are also in good agreement with theoretical values.

Molecular orbital analysis and density of state

Figure 3 shows that the HOMO is located over the C1–C3, C5–C3, C7–C8, and C10–C11 bonds of 3-pmk. On the other side, LUMO orbital is mainly localized over the C8-N15, C7-C10, and C10-O16 bonds. The figure shows that the HOMO has bonding characteristics between the atoms C–C whereas the LUMO has antibonding character between the C–N, and C–O bonds. Consequently, the HOMO/LUMO transition implies an electron density transfer to the C–O bond of the ethanoyl group and C–N bond from C–C bonds. Moreover, these orbital's significantly overlap in their position for 3-pmk. But, while the HOMO-1 is localized on the whole molecule, LUMO + 1 is localized on the pyridine ring.

The energy gap between the HOMO and LUMO is very important for determining the quantum chemical properties of a molecule. In order to understand various aspects of pharmacological sciences including drug design and the possible eco-toxicological characteristics of the drug molecules, several new chemical reactivity descriptors have been proposed. Conceptual DFT based descriptors have helped in many ways to understand the structure of molecules and their reactivity by calculating the chemical potential, global hardness, and electrophilicity.[20] These quantum chemical properties include electrical properties, kinetic stability, optical polarizability and chemical reactivity descriptors, such as hardness and softness. The concept of hardness (η) is related to a compound's reactivity and is a property that measures the extent of chemical reactivity to which the addition of a charge stabilizes the system. The chemical potential (μ_c) provides a global reactivity index and is related to charge transfer from a system of higher chemical potential to one of lower chemical potential. Electronegativity (χ) is the power to attract electrons which is equal to the negative of the chemical potential. All these properties using information on the energies of HOMO and LUMO can be calculated according to the following simple relations: $I = -E_{HOMO}$, $A = -E_{LUMO}$, $\eta = (-E_{HOMO} + E_{LUMO})/2$ and $\mu = (E_{HOMO} + E_{LUMO})/2$, $\omega = \mu^2/2\eta$.[21]

The energy of the frontier molecular orbitals HOMO and LUMO, HOMO-LUMO energy gaps

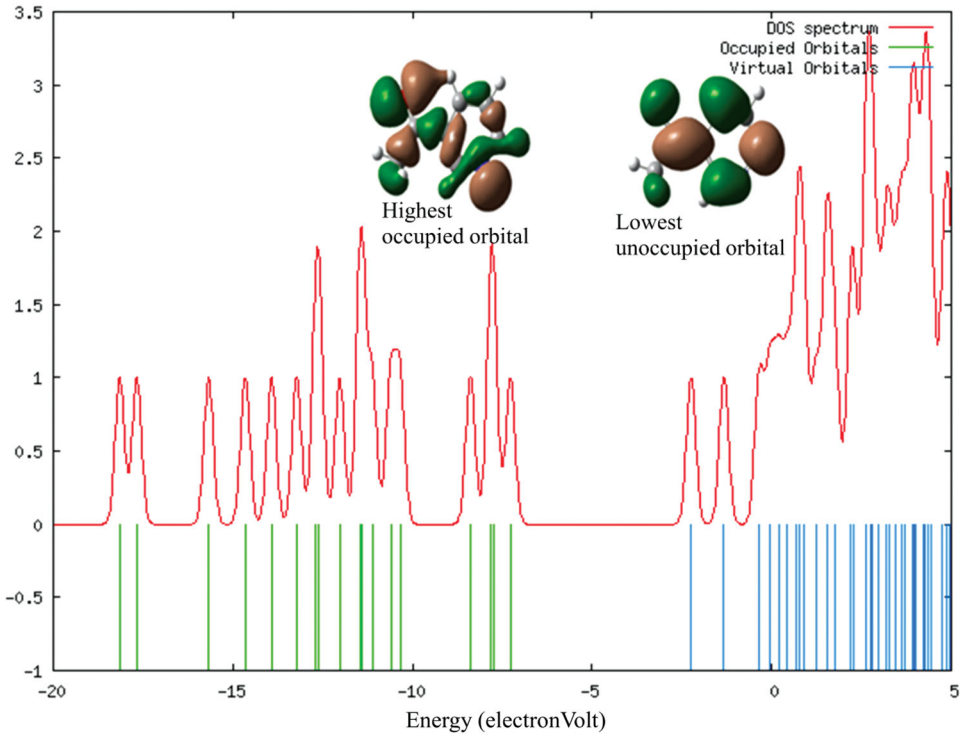

Figure 4. The simulated density of states spectrum of 3-pyridyl methyl ketone molecule. The spectrum lines allow us to see occupied and virtual orbitals more respectively.

and quantum chemical properties (electronegativity, chemical potential, hardness, softness, and global electrophilicity index) for the 3-pmk calculated at B3LYP/6-311++G(d,p) level is listed in Table 3. For the title molecule, HOMO-LUMO gap is equal to 5.03 eV. This value explains the eventual charge transfer interaction with the molecule, which influences the biological activity of the compound. The relatively high value of $\Delta E_{HOMO-LUMO}$ indicates that the title compound presents high chemical stability and it has low reactivity.[20]

The hardness signifies the resistance toward the deformation of electron cloud of chemical systems under small perturbations encountered during chemical process. In terms of chemical hardness, a large HOMO–LUMO energy gap indicates a hard molecule and is related to more stable molecules, whereas a small gap indicates a soft molecule and is related to a more reactive molecule.[20] Soft systems are large and highly polarizable, while hard systems are relatively small and much less polarizable.[20] Chemical hardness, η; Ionization potential, I; and electron affinity, A; are calculated to be 2.15 eV, 7.27 eV, and 2.24 eV, respectively.

The calculated electrophilicity (ω) of the 3-pmk molecule is 5.25 eV. This parameter permits the classification of organic molecules as strong, $\omega > 1.5$ eV, moderate, $0.8 < \omega < 1.5$ eV and marginal electrophiles, $\omega < 0.8$ eV. On the other hand, a good correlation with the inverse of the electrophilicity $(1/\omega)$ can be made, thus molecules located at the bottom of the electrophilicity scale classified as marginal electrophiles corresponds as good nucleophiles.[21,22] Since calculated value of $\omega > 1.5$ eV which is strong, and this value ensures the strong energy transformation between HOMO and LUMO.

The simulated density of states (DOS) spectrum is shown Fig. 4. The density of states indicates the number of available states of the molecular orbitals at different energy of the molecule.[23] DOS spectrum was calculated by Mulliken population analysis and created by convoluting the available energy levels information with Gaussian curves of unit height.[24] The spectrum allows us to see occupied and virtual orbitals more respectively (green and blue lines).

Table 3. The calculated energy gaps and quantum chemical properties (ionization potential, electron affinity, global hardness, electronegativity, chemical potential, global softness, global electrophilicity) of title compound at Density Functional Theory/Becke three Lee-Yang-Parr/6-311++G(d,p).

No	Molecular Orbitals	Energy (eV)		Energy gap (eV)	Ionization potential (I) (eV)	Electron affinity (A) (eV)	Global hardness (η) (eV)	Electronegativity (χ) (eV)	Chemical potential (μ_c) (eV)	Global softness (σ) (eV^{-1})	Global electrophilicity (ω) (eV)
1	H	−7.27	ΔE_{H-L}	5.03	7.27	2.24	2.15	4.75	−4.75	0.23	5.25
	L	−2.24									
2	H-1	−7.75	$\Delta E_{H-1-L+1}$	6.42	7.75	1.33	3.21	4.54	−4.54	0.15	3.21
	L+1	−1.33									
3	H-2	−7.82	$\Delta E_{H-2-L+2}$	7.47	7.82	0.34	3.74	4.08	−4.08	0.13	2.22
	L+2	−0.34									

H: HOMO (Highest Occupied Molecular Orbital); L: LUMO (Lowest Unoccupied Molecular Orbital); eV: electron volt; eV^{-1}: 1/electronVolt.

Molecular electrostatic potential analysis

The molecular electrical potential surfaces (MEP) of 3-pmk were shown in Figs. 5 and 6. This map allows us to visualize variably charged regions of a molecule. The knowledge of the charge distributions can be used to determine how molecules interact with one another and it is also used to determine the nature of the chemical bond. The red and blue region refers to the electron rich and electron poor region while the slightly electron rich region is indicated by yellow and the slightly electron poor region by the light blue region.[17] Figure 5 shows that the pyridine ring (except its nitrogen atom) is which the color is neither red nor blue, but almost neutral. The region around the oxygen atom of the ethanoyl group was found to be electron rich (red), which is due to the lone pair of oxygen atom. The region around the nitrogen atom was found to be electron deficient (yellow) because the electronegative nitrogen atom soaks up the electrons in the hydrogen atoms. The region around the nitrogen atom of the pyridine ring was found to be slightly electron rich. The color code of these maps is in the range between −0.046 (deepest red) and 0.046 arbitrary units (a.u.) (deepest blue) in the compound.

Thermodynamic properties

The thermodynamic functions were derived by means of the vibrational analysis with 6-311++G (d,p) basis set in gas phase. The temperature variations of the heat capacity at constant pressure (Cp), entropy (S), enthalpy changes (ΔH), and Gibbs free energies for 3-pyridyl methyl ketone are presented in Fig. 7. The values of the calculated thermodynamic functions over the temperature range 100–1000 K are tabulated in Table 4. On the basis of vibration analysis, the statically thermodynamic functions: heat capacity (Cp), entropy (S), enthalpy changes (ΔH), and Gibbs free energy (G) for the title molecule obtained from the theoretical thermodynamic parameters are also listed in Table 4.

The research focus of some thermo molecular characteristics such as zero-point vibrational energy, enthalpy, Gibb's free energy, entropy,

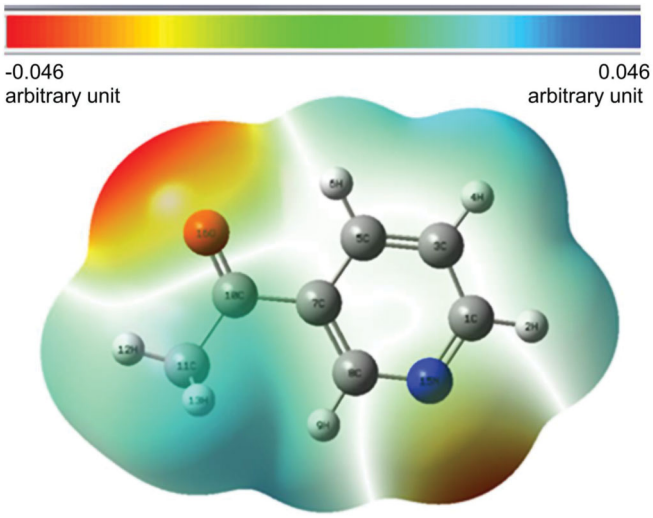

Figure 5. Molecular electrostatic potential surface for 3-pyridyl methyl ketone in gas phase. This map allows us to visualize variably charged regions of the title molecule.

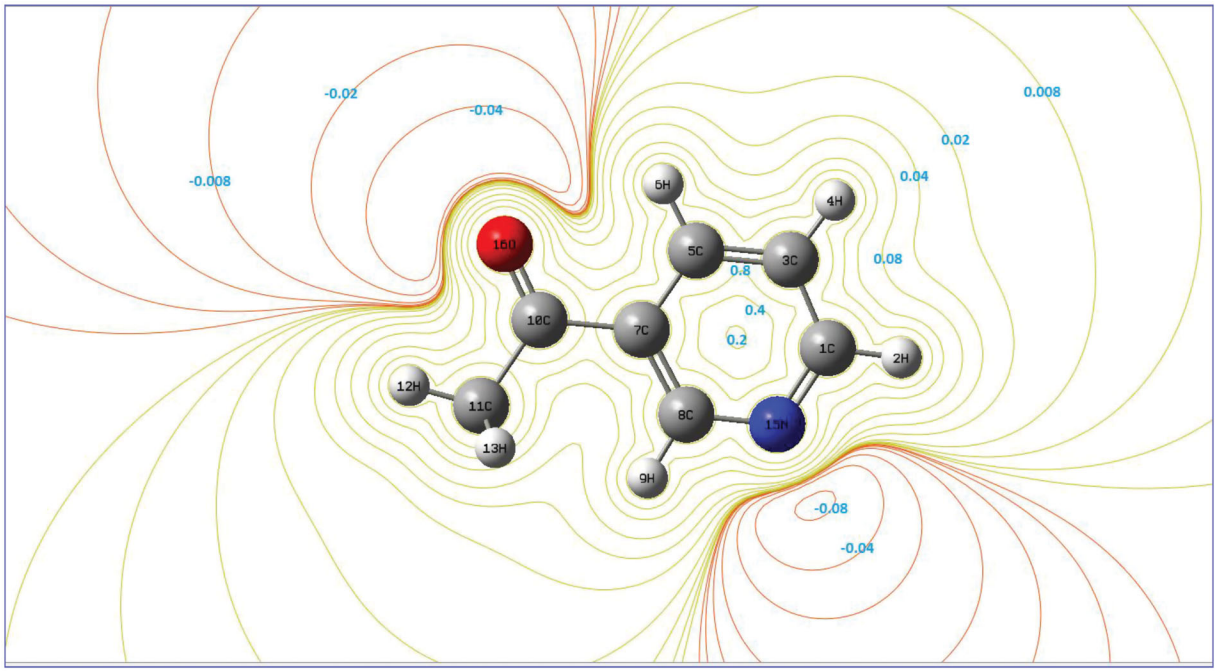

Figure 6. Two dimensions contour map of molecular electrostatic potential surface values (all in arbitrary unit) for 3-pyridyl methyl ketone. The region around the nitrogen atom of the pyridine ring was found to be slightly electron rich.

heat capacity, thermal energy and the partition functions, etc. have been found to play crucial role in the material characterization and to understand the reactivity or mode of action and environmental influences on the molecules.[25] The molecules taken for this investigation possess a remarkable interest in thermodynamic property analysis. Since it is a characteristic property of the molecule, the zero-point vibrational energy remains constant at all the temperatures. The zero-point vibrational energy obtained for structure optimization of 3-pmk has been calculated to 0.1242854 a.u. The thermodynamic data reveal helpful information for the further studies on the title compounds when they are seen as a reactant to take part in a new reaction. Apparently, all of the analyzed thermodynamic parameters showed an increase in line with the temperature while G is observed to decrease with T (Fig. 7) which is due to the rise of molecular vibrations with temperature rise. The entropy and enthalpy changes showed that the molecule

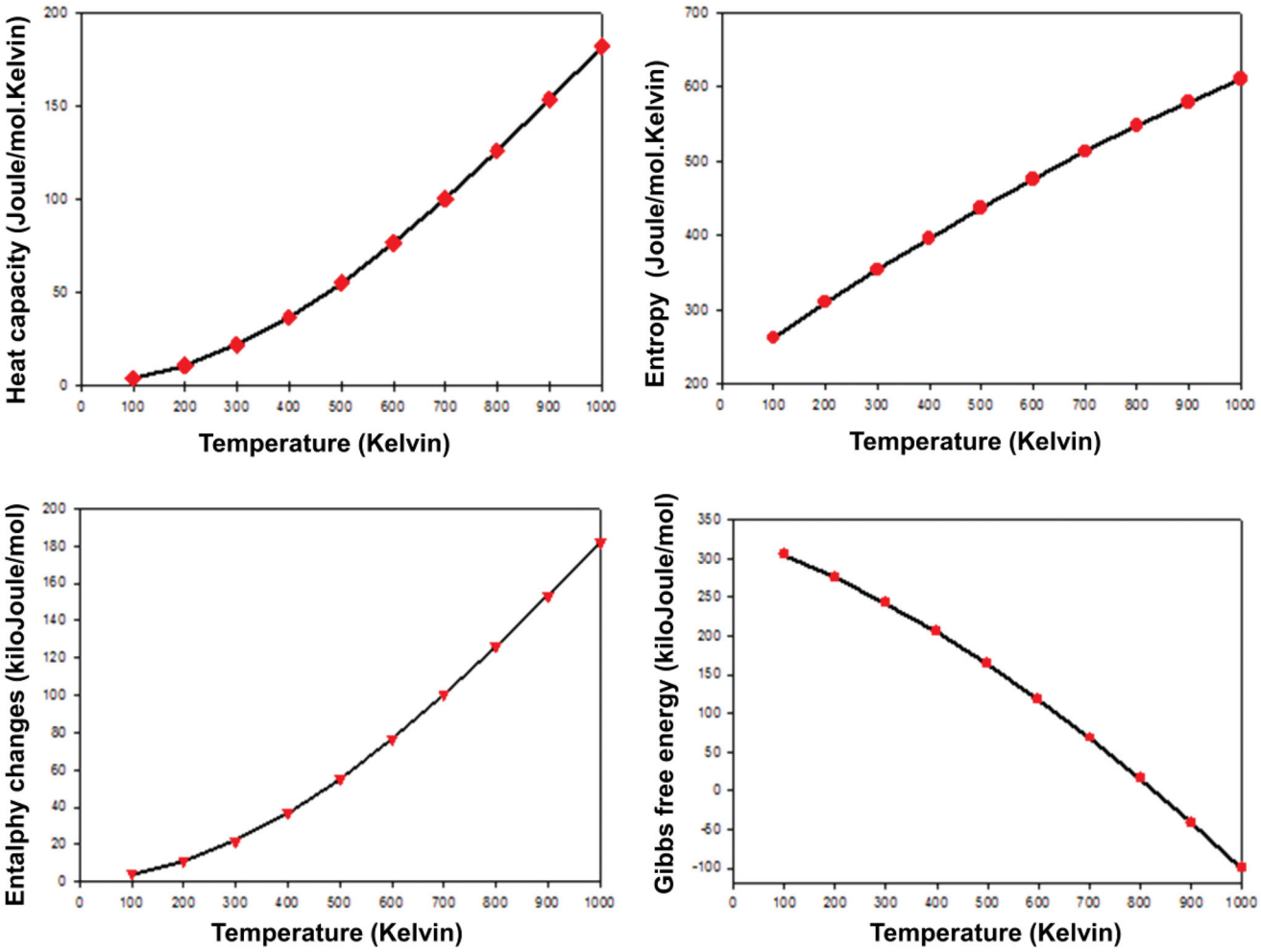

Figure 7. Thermodynamic properties (heat capacity, entropy, entalphy changes, and Gibbs free energy) of 3-pyridyl methyl ketone as a function of temperature in the range 100–1000 Kelvin. Gibbs free energy gradually diminishes along with the rise of temperature. The entropy and constant-volume specific heat capacity increase in the selected temperature ranges.

Table 4. Thermodynamic properties (heat capacity, entropy, enthalpy changes, Gibbs free energy, zero-point energy) at different temperatures in the range 100–1000 Kelvin of 3-pyridyl methyl ketone computed at the Becke three Lee-Yang-Parr/6-311++G(d,p) level.

Temperature (K)	$C^0_{p,m}$ (J mol^{-1} K^{-1})	S^0_m (J mol^{-1} K^{-1})	ΔH^0_m (kJ mol^{-1})	G_{corr} (kJ mol^{-1})	ε_{ZPE} (kJ mol^{-1})
100	45.86	262.20	4.01	304.12	326.31
200	81.27	310.41	11.17	275.43	326.31
300	120.60	354.08	22.07	242.21	326.31
400	158.90	396.51	36.92	204.70	326.31
500	191.65	437.47	55.33	163.01	326.31
600	218.22	476.36	76.70	117.33	326.31
700	239.70	512.95	100.47	67.88	326.31
800	257.28	547.26	126.18	14.88	326.31
900	271.88	579.41	153.50	−41.42	326.31
1000	284.13	609.60	182.14	−100.85	326.31

J: Joule; K: Kelvin; $C^0_{p,m}$: heat capacity; S^0_m : entropy; ΔH^0_m : entalphy changes; G_{corr} : Gibbs free energy, ε_{ZPE} : zero-point energy.

has more flexibility of variating its own thermodynamic system with respect to the temperature. All the thermomolecular data revealed the crucial and helpful information for the further studies on the 3-pmk. They can be used to compute the other thermodynamic characteristics according to relationships of thermodynamical parameters and estimate directions of chemical reactions in line with the second law of thermodynamics in thermo chemical fields.

Gibbs free energy (G) is also a critical thermodynamic quantity. The change of G can be used

to determine not only the stability of the product but also the direction of the reaction throughout the hydriding/dehydriding reaction. Admittedly, the G can be defined by the formula put below,[26]

$$G = H - TS \quad (1)$$

where T, S are the temperature and entropy. H is enthalpy and internal energy (E), which can be expressed as

$$H = E + PV \quad (2)$$

so;

$$G = E - TS + PV \quad (3)$$

where P and V are pressure and volume, respectively. For solid and liquid phase, the value of PV is far less than that of Gibbs free energy at atmospheric pressure which means that PV can be ignored. Thus, the G can be attained from the formula expressed below;

$$G = E - TS \quad (4)$$

The relations between the calculated Gibbs free energy and the temperature are presented in Fig. 7. Results pointed out that Gibbs free energy gradually diminishes along with the rise of temperature. In other words, while the entropy and constant-volume specific heat capacity increase in the selected temperature ranges, the calculated values of Gibbs free energy diminishes.

Fukui functions

According to Fukui's Frontier Molecular Orbital Theory, the chemical reactivity of the molecule in terms of HOMO or LUMO electron density is interpreted.

Fukui functions are evaluated using the finite difference (FD) methodology for the neutral molecule and for the cationic and anionic structure with the same molecular geometry.

In FD calculations, three types of Fukui functions were introduced.[27]

$$f_k^+ = q_k(N+1) - q_k(N) \text{ for nucleophilic attack} \quad (5)$$

$$f_k^- = q_k(N) - q_k(N-1) \text{ for electrophilic attack} \quad (6)$$

$$f_k^0 = (1/2)\ [q_k(N+1) - q_k(N-1)] \text{ for neutral (radical) attack} \quad (7)$$

Table 5. Condensed Fukui functions (nucleophilic attack, electrophilic attack, neutral attack) of 3-pyridyl methyl ketone calculated from Hirshfeld charges.

Atoms	f^+	f^-	f^0	f^+/f^-	f^-/f^+
C_1	0.0688	0.1152	0.0920	0.5966	1.6761
H_2	0.0527	0.0535	0.0531	0.9839	1.0164
C_3	0.0546	0.0549	0.0547	0.9943	1.0736
H_{13}	0.0333	0.0354	0.0344	0.9389	1.0651
H_{14}	0.0333	0.0357	0.0345	0.9342	1.0704
C_5	0.0469	0.0747	0.0608	0.6276	1.5933
H_6	0.0331	0.0407	0.0369	0.8123	1.2310
C_7	0.0360	0.0510	0.0435	0.7056	1.4173
C_{10}	0.0622	0.1227	0.0925	0.5070	1.9722
H_4	0.0379	0.0407	0.0393	0.9314	1.0736
C_8	0.0561	0.0582	0.0571	0.9633	1.0381
H_{12}	0.0336	0.0332	0.0334	1.0101	0.9900
H_9	0.0444	0.0304	0.0374	1.4602	0.6849
C_{11}	0.0434	0.0308	0.0371	1.4105	0.7090
N_{15}	0.1674	−0.4521	−0.1424	−0.3702	−2.7013
O_{16}	0.1969	0.1525	0.1747	1.2913	0.7744

f^+: nucleophilic attack; f^-: electrophilic attack; f^0: neutral (radical) attack.

In these equations, q_k is the atomic charge at the rth atomic site is the neutral (N), anionic ($N+1$), cationic ($N-1$) chemical species.[28,29] As Roy et al. presented, the highest value of the $\left(f_k^+/f_k^-\right)$ ratio is relative electrophilicity and the highest value of the $\left(f_k^-/f_k^+\right)$ ratio is relative nucleophilicity.[30] The data of the Fukui functions are listed in Table 5. The maximum value of the electrophilic reactivity descriptors was determined at H_9 atom, while the maximum value of the nucleophilic reactivity descriptors at atoms was predicted at C_{10} atoms. So, the behavior of molecule as nucleophilic (C_1, C_3, C_5, C_7, C_8, C_{10}, H_2, H_6, H_4, H_{13}, and H_{14}) and electrophilic (N_{15}, C_{11}, H_{12}, H_9, and O_{16}) attack during reaction depends on the local behavior of molecule.[31]

Non-linear optical properties

Non-linear optical properties (NLO) activity arises from the interactions of electromagnetic fields in different media to produce fields changed in phase, frequency, amplitude, or other propagation characteristics.[32]

In this study, dipole moment, polarizability, and the first-order hyperpolarizability of the 3-pmk along with related properties (μ, $\overline{\alpha}$, and $\Delta\alpha$) are calculated by using DFT/B3LYP method with 6-311 G++(d, p) basis set. The data of the non-linear optical properties were listed in Table 6. The first-order hyperpolarizability (β_0) is a third rank tensor that can be described by a $3 \times 3 \times 3$

Table 6. The electric dipole moment μ (Debye), average polarizability $\bar{\alpha}$, anisotropy of polarizability $\Delta\alpha$ ($10^{-24}esu$), and first hyperpolarizability β_0 ($10^{-30}esu$) of the title molecule.

Dipole moment		Polarizability		First hyperpolarizability			
μ_x	1.02	α_{xx}	17.51	β_{xxx}	−2.35	β_x	−1.79
μ_y	−0.53	α_{yx}	−0.23	β_{xxy}	−0.27	β_y	−0.51
μ_z	0.11	α_{yy}	13.05	B_{yxy}	0.49	β_z	−0.83
μ	1.15	α_{zx}	2.39	β_{yyy}	−0.20	β_{tot}	2.04
		α_{zy}	2.86	β_{xxz}	−0.91	β	−0.49
		α_{zz}	10.12	B_{yxz}	0.06		
		$\bar{\alpha}$	13.56	β_{yyz}	0.07		
		$\Delta\alpha$	9.13	B_{zxz}	0.07		
				B_{zyz}	−0.04		
				β_{zzz}	0.01		

matrix. The 27 components of the 3D matrix can be reduced to 10 components because of the Kleinman symmetry.[33,34]

Expressions used for the calculations are given below:

$$E = E^0 - \mu_\alpha F_\alpha - \frac{1}{2}\alpha_{\alpha\beta}F_\alpha F_\beta - \frac{1}{6}\beta_{\alpha\beta\gamma}F_\alpha F_\beta F_\gamma + \cdots\cdots \quad (8)$$

where E^0 is the energy with no field present and F_α are the components of the applied field. The permanent dipole moment (μ), the mean polarizability ($\overline{\alpha}$), the anisotropy of the polarizability ($\Delta\alpha$), and the first order hyperpolarizability (β_0) by using the component x, y, z are given bellow.[35,36]

$$\mu^2 = \mu_x^2 + \mu_y^2 + \mu_z^2 \quad (9)$$

$$\overline{\alpha} = (\alpha_{xx} + \alpha_{yy} + \alpha_{zz})/3 \quad (10)$$

$$\Delta\alpha = \frac{1}{\sqrt{2}}\left[(\alpha_{xx}-\alpha_{yy})^2 + (\alpha_{yy}-\alpha_{zz})^2 + (\alpha_{zz}-\alpha_{xx})^2 + 6(\alpha_{xy}^2 + \alpha_{yz}^2 + \alpha_{xz}^2)\right]^{1/2} \quad (11)$$

$$\beta_0 = \left[(\beta_{xxx} + \beta_{xyy} + \beta_{xzz})^2 + (\beta_{yyy} + \beta_{xxy} + \beta_{yzz})^2 + (\beta_{zzz} + \beta_{xxz} + \beta_{yyz})^2\right]^{1/2} \quad (12)$$

Urea is the prototypical molecule used in analyzing of the NLO characteristic of the compound. So, urea was used often as a brink value for comparing with another. Theoretically, the first hyperpolarizability of the 3-pmk is 5,5 times greater than that of urea (β_0 of urea is 0.3728×10^{-30} *esu*).[37] Therefore, investigated molecule will show a little more non-linear optical response and might be used as non-linear optical (NLO) material.[31,36,38]

Charge analysis

Examining molecular orbitals gives information about the reactivity of molecules. The electronic charges of the atoms define the bonding potential of a molecule. Because atomic charges affect the molecular moment, molecular polarity, electronic structure, and many other properties, charge density values have an important place in quantum chemical calculations. The capability of the atoms to bond was investigated by calculating the charge distribution of the optimized structure. NBO, Hirshfeld, and APT charges were calculated by determining the electron population of each atom as defined by the 6-311 g++(d,p) basis set. The calculated charge values are tabulated in Table 7 and presented in Fig. 8. The magnitude of the carbon atomic charge is found to be positive and negative. All the charge of the carbon atoms (C_1, C_8, and C_{10}) attached to the electronegative atoms have positive due to their attachment to the electronegative oxygen and nitrogen atoms.[39,40] These electronegative atoms pulled out the partial charges from the carbon atom and therefore they became positive. The negative charge values observed in N_{15}, C_3, C_5, C_7, C_{11}, and O_{16}. The positive charge values observed in C_1, C_8, C_{10}, H_2, H_4, H_6, H_9, H_{12}, H_{13}, and H_{14}.

Conclusion

A complete structural, vibrational, thermodynamic, electronic, nonlinear optical investigation along with FT-IR (mid and Far-IR) analysis of 3-pyridyl methyl ketone have been carried out with DFT (B3LYP) using 6-311++G(d,p) basis set. The FT-IR (mid and far IR) bands of 3-pyridyl methyl ketone were also recorded and compared with the theoretical data. Detailed assignments were made based on TED analysis. A comparison of the results of experimental and theoretical study gave a full description of the vibrational properties of the title molecule. The HOMO–LUMO energy gap is calculated to be 5.03 eV. That is to say, this molecule has a high kinetic stability, and low chemical reactivity. It was determined by MEP analysis that the electron charge density of the molecule was high around the nitrogen and oxygen atom of ethanoyl group,

Table 7. Comparison of Natural Bond Orbital, Hirshfeld and Atomic Polar Tensor atomic charges values(all in electron charge) for 3-pyridyl methyl ketone at Becke three Lee-Yang-Parr method with 6-311++G(d,p) basis set.

Atoms	Atomic polar tensor	Natural bond orbital	Hirshfeld	Atoms	Atomic polar tensor	Natural bond orbital	Hirshfeld
C_1	0.234	0.074	0.040	H_9	0.035	0.202	0.058
H_2	0.026	0.194	0.061	C_{10}	0.997	0.555	0.164
C_3	−0.144	−0.237	−0.041	C_{11}	−0.127	−0.670	−0.097
H_4	0.041	0.214	0.056	H_{12}	0.023	0.234	0.054
C_5	0.097	−0.119	−0.009	H_{13}	0.023	0.225	0.053
H_6	0.088	0.237	0.061	H_{14}	0.023	0.225	0.053
C_7	−0.336	−0.184	−0.019	N_{15}	−0.447	−0.461	−0.198
C_8	0.214	0.074	0.034	O_{16}	−0.747	−0.562	−0.270

The electronic charges of the atoms define the bonding potential of a molecule. In Natural bond orbital analysis, orbitals are orthogonalized and localized to form one or two center orbitals. These orbitals are classified as core orbitals. Hirshfeld atomic charge analysis based on electron density; each atom's charge is obtained by integrating the electron density over its volume. Atomic polar tensor analysis is defined using tensor of dipole moment of a molecule.

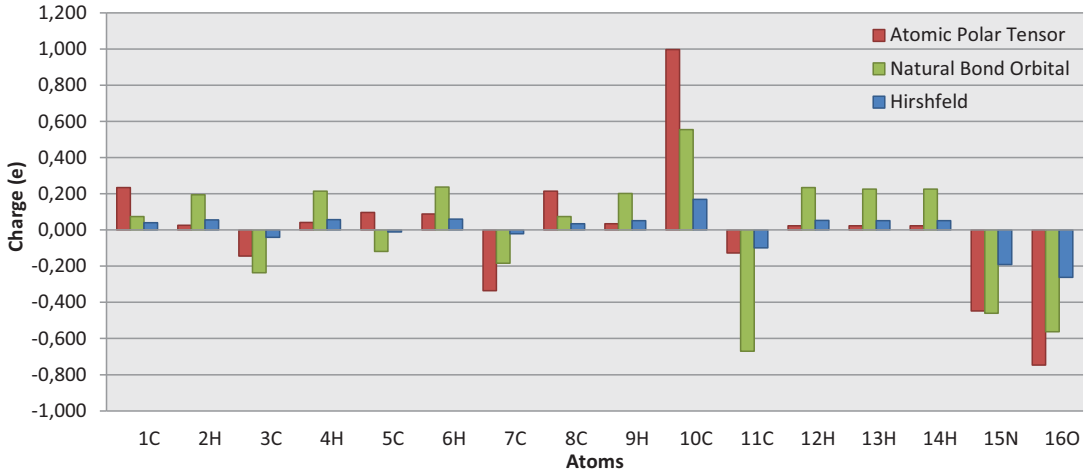

Figure 8. Natural Bond Orbital, Hirshfeld and Atomic Polar Tensor electron charge distribution for 3-pyridyl methyl ketone. *The electronic charges of the atoms define the bonding potential of a molecule. In Natural Bond Orbital analysis, orbitals are orthogonalized and localized to form one or two center orbitals. These orbitals are classified as core orbitals. Hirshfeld atomic charge analysis based on electron density; each atom's charge is obtained by integrating the electron density over its volume. Atomic Polar Tensor analysis is defined using atomic polar tensor of a molecule.

and low around the hydrogen atoms. Some thermodynamic parameters at different temperature values were examined. Apparently, all of the analyzed thermodynamic parameters showed an increase in line with the temperature while G is observed to decrease with T, which is due to the rise of molecular vibrations with temperature rise. The entropy and enthalpy changes showed that the molecule has more flexibility of variating its own thermodynamic system with respect to the temperature. The dipole moment, polarizability and first-order hyperpolarizability of the molecule were theoretically calculated and compared with the values of the urea molecule. The first hyperpolarizability of the 3-pmk is 5,5 times greater than that of urea. Therefore, investigated molecule will show a little non-linear optical response and might be used as non-linear optical (NLO) material.

Acknowledgment

The authors would like to thank the reviewers for their comments that help improve the manuscript.

References

[1] Wecker, L.; Marrero-Rosado, B.; Engberg, M. E.; Johns, B. E.; Philpot, R. M. 3-Acetylpyridine Neurotoxicity in Mice. *Neurotoxicology* **2017**, *58*, 143–152. DOI: 10.1016/j.neuro.2016.11.010.

[2] Agustin, B.; Lin, S.-Y.; Kurniawan, A.; Ju, Y.-H.; Soetaredjo, F. E.; Ismadji, S. Solubilities of 3-Acetylpyridine in Supercritical Carbon Dioxide at Several Temperatures and Pressures: Experimental and Modeling. *Fluid Phase Equilibria* **2013**, *354*, 127–132. DOI: 10.1016/j.fluid.2013.06.036.

[3] Zhai, C.; Cui, F.; Liu, X. A Combined Experimental and Theoretical Study on Vibrational Spectra of 2-Acetylpyridine. *Spectrochimica Acta Part A: Molecular and Biomolecular Spectroscopy* **2015**, *134*, 90–95. DOI: 10.1016/j.saa.2014.06.086.

[4] Uwai, K.; Konno, N.; Kitamura, S.; Ohta, S.; Takeshita, M. Purification and Characterization of Rat Liver Enzyme Catalyzing Stereoselective Reduction of Acetylpyridines. *Chirality* **2005**, *17*, 494–500. DOI: 10.1002/chir.20197.

[5] Sarkar, S. K.; Ghoshal, G.; Kastha, S. Effect of Ring Aza Substitution on the Luminescence of Aromatic Ketones Luminescence of Isomeric Acetylpyridines. *Chemical Science* **1983**, *92*, 47–58.

[6] Medhi, K. C. The Vibrational Spectra of 2-, 3-and 4-Acetylpyridine. *Indian Journal of Physics* **1977**, *51A*, 399–413.

[7] Sett, P.; Chattopadhyay, S.; Mallick, P. K. Normal Coordinate Analyses of Three Isomeric Acetylpyridines and Acetophenone. *Journal of Raman Spectroscopy* **2000**, *31*, 177–184. DOI: 10.1002/(SICI)1097-4555(200003)31:3<177::AID-JRS509>3.0.CO;2-K.

[8] Frisch, M. J.; Trucks, G.; Schlegel, H.; Scuseria, G.; Robb, M.; Cheeseman, J.; Barone, V.; Mennucci, B.; Petersson, G.; et.al. *Gaussian 09. Revision C.01*; Gaussian, Inc.: Wallingford CT, 2009.

[9] Becke, A. D. Density-Functional Thermochemistry. III. The Role of Exact Exchange. *The Journal of Chemical Physics* **1993**, *98*, 5648–5652. DOI: 10.1063/1.464913.

[10] Lee, C.; Yang, W.; Parr, R. G. Development of the Colle-Salvetti Correlation-Energy Formula into a Functional of the Electron Density. *Physical Review. B* **1988**, *37*, 785–789. DOI: 10.1103/PhysRevB.37.785.

[11] Pulay, P.; Baker, J.; Wolinski, J. K. *PQS, Version 3.3, Parallel Quantum Solutions, Green Acres Road*; Fayetteville, Arkansas, 2007, 72703 pp.

[12] Werner, J.; Boeckmann, J.; Nather, C. Investigations on the Structure Diversity and Thermal Degradation Behavior of Cd^{II} and Zn^{II} Thiocyanato Coordination Compounds Based on 3-Acetylpyridine as Neutral Co-Ligand. *Zeitschrift für Anorganische und Allgemeine Chemie* **2012**, *638*, 2257–2264. DOI: 10.1002/zaac.201200268.

[13] Rached, A. B.; Maalej, W.; Guionneau, P.; Daro, N.; Mhiri, T.; Feki, H.; Elaoud, Z. Synthesis, Crystal Structure, and Vibrational and DFT Simulation Studies of Benzylammonium Dihydrogen Phosphate. *Journal of Physics and Chemistry of Solids* **2018**, *123*, 150–156. DOI: 10.1016/j.jpcs.2018.07.017.

[14] Merrick, P. J.; Moran, D.; Radom, L. An Evaluation of Harmonic Vibrational Frequency Scale Factors. *Journal of Physical Chemistry. A* **2007**, *111*, 11683–11700. DOI: 10.1021/jp073974n.

[15] Balachandran, V.; Rajeswari, S.; Lalitha, S. Thermal and Magnetic Properties and Vibrational Analysis of 4-(Dimethylamino) Pyridine. A Quantum Chemical Approach. *Spectrochimica Acta Part A: Molecular and Biomolecular Spectroscopy* **2014**, *124*, 277–284. DOI: 10.1016/j.saa.2014.01.023.

[16] Yurdakul, Ş.; Badoğlu, S.; Güleşci, Y. Experimental and Theoretical Study on Free 5-Nitroquinoline, 5-Nitroisoquinoline, and Their Zinc (II) Halide Complexes. *Spectrochimica Acta Part A: Molecular and Biomolecular Spectroscopy* **2015**, *137*, 945–956. DOI: 10.1016/j.saa.2014.08.097.

[17] Xavier, S.; Periandy, S.; Carthigayan, K.; Sebastian, S. Molecular Docking, TG/DTA, Molecular Structure, Harmonic Vibrational Frequencies, Natural Bond Orbital and TD-DFT Analysis of Diphenyl Carbonate by DFT Approach. *Journal of Molecular Structure* **2016**, *1125*, 204–216. DOI: 10.1016/j.molstruc.2016.06.071.

[18] Al-Tamimi, A.-M. S.; MaryAl, T. Y. S.; Hassan, H. M.; Resmi, K. S.; El-Emam, A. A.; Narayana, B.; Sarojini, B. K. Study on the Structure, Vibrational Analysis and Molecular Docking of Fluorophenyl Derivatives Using FT-IR and Density Functional Theory Computations. *Journal of Molecular Structure* **2018**, *1164*, 172–179. DOI: 10.1016/j.molstruc.2018.03.070.

[19] Selvaraj, S.; Rajkumar, P.; Kesavan, M.; Gunasekaran, S.; Kumaresan, S. Experimental and Theoretical Investigations on Spectroscopic Properties of Tropicamide. *Journal of Molecular Structure* **2018**, *1173*, 52–62. DOI: 10.1016/j.molstruc.2018.06.097.

[20] Rocha, M.; Di Santo, A.; Arias, J. M.; Gil, D. M.; Altabef, A. B. Ab-Initio and DFT Calculations on Molecular Structure, NBO, HOMO–LUMO Study and a New Vibrational Analysis of 4-(Dimethylamino) Benzaldehyde. *Spectrochimica Acta Part A: Molecular and Biomolecular Spectroscopy* **2015**, *136*, 635–643. DOI: 10.1016/j.saa.2014.09.077.

[21] Sureshkumar, B.; Mary, Y. S.; Resmi, K. S.; Panicker, C. Y.; Armaković, S.; Armaković, S. J.; Van Alsenoy, C.; Narayana, B.; Suma, S. Spectroscopic Analysis of 8-Hydroxyquinoline Derivatives and Investigation of Its Reactive Properties by DFT and Molecular Dynamics Simulations. *Journal of Molecular Structure* **2018**, *1156*, 336–347. DOI: 10.1016/j.molstruc.2017.11.120.

[22] Costa, R. A.; Oliveira, K. M. T.; Costa, E. V.; Pinheiro, M. L. B. Vibrational, Structural and Electronic Properties Investigation by DFT Calculations and Molecular Docking Studies with DNA Topoisomerase II of Strychnobrasiline Type Alkaloids: A Theoretical Approach for Potentially Bioactive Molecules. *Journal of Molecular Structure* **2017**, *1145*, 254–267. DOI: 10.1016/j.molstruc.2017.05.087.

[23] Shah, T. A.; Alam, U.; Alam, M. U.; Park, S.; Muneer, M. Single Crystal X-Ray Structure, Spectroscopic and DFT Studies of Imidazo[2,1-b]thiazole: 2-(3-Hydroxy-3-phenylimidazo[2,1-b]thiazol2(3H)-ylidene)-1-phenylethanone. *Journal of Molecular Structure* **2018**, *1157*, 638–653. DOI: 10.1016/j.molstruc.2017.12.074.

[24] Asath, R. M.; Premkumar, S.; Mathavan, T.; Benial, A. M. F. Vibrational Spectroscopic,Molecular Docking, and Quantum Chemical Studies on 6-Aminonicotinamide. *Journal of Molecular Structure* **2017**, *1134*, 143–156. DOI: 10.1016/j.molstruc.2016.12.058.

[25] Hellal, A.; Rachida, D.; Zaout, S.; Elkolli, M.; Chafaa, S.; Touafri, L.; Chafai, N.; Mehri, M.; Benbougerra, K. Structural, Electronic, Vibrational, Optical and Thermodynamic Properties of 3-Oxo-3-p-tolylpropylphosphonic Acid and 4-Oxo-4-ptolyl-butyric Acid: Density Functional Theory Study. *Journal of Molecular Structure* **2018**, *1171*, 527–540. DOI: 10.1016/j.molstruc.2018.06.012.

[26] Liu, J.; Han, H.; Zhang, X.; Li, S.; Ge, S.; Zhang, G.; Gao, T. First-Principles Study the Structural, Electronic, Vibrational and Thermodynamic Properties of Zr1-HfxCoH3. *International Journal of Hydrogen Energy* **2018**, *43*, 19152–19163. DOI: 10.1016/j.ijhydene.2018.08.130.

[27] Bultinck, P.; Carbo-Dorca, R.; Langenaeker, W. Negative Fukui Functions: New Insights Based on Electronegativity Equalization. *Journal of Chemical Physics* **2003**, *118*, 4349–4356. DOI: 10.1063/1.1542875.

[28] Yang, W.; Mortier, W. J. The Use of Global and Local Molecular Parameters for the Analysis of the Gas-Phase Basicity of Amines. *Journal of American Chemical Society* **1986**, *108*, 5708–5711. DOI: 10.1021/ja00279a008.

[29] Parr, R. G.; Yang, W. Density Functional Approach to the Frontier-Electron Theory of Chemical Reactivity. *Journal of American Chemical Society* **1984**, *106*, 4049–4050. DOI: 10.1021/ja00326a036.

[30] Roy, R. K.; Krishnamurti, S.; Geerlings, P.; Pal, S. Local Softness and Hardness Based Reactivity Descriptors for Predicting Intra- and Intermolecular Reactivity Sequences: Carbonyl Compounds. *Journal of Physical Chemistry A* **1998**, *102*, 3746–3755. DOI: 10.1021/jp973450v.

[31] Srivastava, S.; Gupta, P.; Sethi, A.; Singh, R. P. One Pot Synthesis of Curcumin-NSAIDs Prodrug, Spectroscopic Characterization, Conformational Analysis, Chemical Reactivity, Intramolecular Interactions and First Order Hyperpolarizability by DFT Method. *Journal of Molecular Structure* **2016**, *1117*, 173–180. DOI: 10.1016/j.molstruc.2016.03.033.

[32] Raja, M.; Raj Muhamed, R.; Muthu, S.; Suresh, M. Synthesis, Spectroscopic (FT-IR, FT-Raman, NMR, UV-Visible), First Order Hyperpolarizability, NBO and Molecular Docking Study of (E)-1-(4-Bromobenzylidene)Semicarbazide. *Journal of Molecular Structure* **2017**, *1128*, 481–492. DOI: 10.1016/j.molstruc.2016.09.017.

[33] Sajan, D.; Joe, D. H.; Jayakumar, V. S.; Zaleski, J. Structural and Electronic Contributions to Hyperpolarizability in Methyl p-Hydroxy Benzoate. *Journal of Molecular Structure* **2006**, *785*, 43–53. DOI: 10.1016/j.molstruc.2005.09.041.

[34] Kleinman, D. A. Nonlinear Dielectric Polarization in Optical Media. *Physical Review* **1962**, *126*, 1977–1979. DOI: 10.1103/PhysRev.126.1977.

[35] Zhang, R.; Du, B.; Sun, G.; Sun, Y. Experimental and Theoretical Studies on *o*-, *m*- and *p*-Chlorobenzylideneaminoantipyrines. *Spectrochimica Acta Part A: Molecular and Biomolecular Spectroscopy* **2010**, *75A*, 1115–1124. DOI: 10.1016/j.saa.2009.12.067.

[36] Karamanis, P.; Pouchan, C.; Maroulis, G. Structure, Stability, Dipole Polarizability and Differential Polarizability in Small Gallium Arsenide Clusters from All-Electron *Ab Initio* and Density-Functional-Theory Calculations. *Physical Review A* **2008**, *77*, 013201. DOI: 10.1103/PhysRevA.77.013201.

[37] Sethi, A.; Singh, R. P.; Shukla, D.; Singh, P. Synthesis of Novel Pregnane-Diosgenin Prodrugs via Ring a and Ring a Connection: A Combined Experimental and Theoretical Studies. *Journal of Molecular Structure* **2016**, *1125*, 616–623. DOI: 10.1016/j.molstruc.2016.07.020.

[38] Eryılmaz, S.; Akdemir, N.; İnkaya, E. The Examination of Molecular Structure Properties of 4,4'-Oxydiphthalonitrile Compound: Combined Spectral and Computational Analysis Approaches. *Spectroscopy Letters* **2019**, *52*, 28–42. DOI: 10.1080/00387010.2018.1544569.

[39] Yurdakul, Ş.; Temel, E.; Büyükgüngör, O. Crystal Structure, Spectroscopic Characterization, Thermal Properties and Theoretical Investigations on [Ag(methyl 4-pyridyl ketone)2NO_3]. *Journal of Molecular Structure* **2019**, *1191*, 301–313. DOI: 10.1016/j.molstruc.2019.04.071.

[40] Büyükmurat, Y.; Akyüz, S. Theoretical and Experimental IR Spectra and Assignments of 3-Aminopyridine. *Journal of Molecular Structure* **2001**, *563-564*, 545–550. DOI: 10.1016/S0022-2860(00)00801-2.